

Flexural behavior of sandwich beams with novel triaxially woven fabric composite skins

M.Y. Al-Fasih¹, A.B.H. Kueh² and M.H.W. Ibrahim^{*1}

¹Jamilus Research Centre, Faculty of Civil Engineering and Built Environment,
Universiti Tun Hussein Onn Malaysia, 86400 Parit Raja, Johor, Malaysia

²Department of Civil Engineering, Faculty of Engineering, Universiti Malaysia Sarawak, 94300 Kota Samarahan, Sarawak, Malaysia

(Received October 12, 2019, Revised December 12, 2019, Accepted December 20, 2019)

Abstract. This study aims to carry out the experimental and numerical investigation on the flexural behavior of sandwich honeycomb composite (SHC) beams reinforced with novel triaxially woven fabric composite skins. Different stacking sequences of the carbon fiber reinforcement polymer (CFRP) laminate; i.e., 0°-direction of TW (TW0), 0°-direction of UD (UD0), and 90°-direction of UD (UD90) were studied, from which the flexural behavior of SHC beam behaviors reinforced with TW0/UD0 or TW0/UD90 novel laminated skins were compared with those reinforced with UD0/90 conventional laminated skins under four-point loading. Generally, TW0/UD0 SHC beams displayed the same flexural stiffness as UD0/90 SHC beams in terms of load-deflection relationships. In contrast, TW0/UD90 SHC beams showed a 70% lower efficiency than those of UD0/90 SHC. Hence, the TW0/UD0 laminate arrangement is more effective with a mass reduction of 39% compared with UD0/90 for SHC beams, although their stiffness and shear strength are practically identical.

Keywords: flexural behavior; sandwich honeycomb composite; carbon fiber reinforced polymer; unidirectional; triaxial woven fabric

1. Introduction

Great effort has been expended in recent decades in the search for a suitable material that is able to meet the requirements of structures with high performance, while lightweight for various possible applications. Such applications are not only limited to the aerospace industry but also to areas such as building and highway, marine, space exploration, automobile, and sport. The desire to meet the expectations of such widespread applications brings us to the wonders of composite sandwich structures, which is a structure consisted of the core material sandwiched between two skins (He and Hu 2008). The concept of the sandwich structural offers high strength to weight ratio and high bending stiffness to the component of the structures (Belouettar *et al.* 2009). The skins are exposed to tension or compression with the main role of controlling the strength and flexural stiffness of the sandwich structure. On the other hand, the core material mainly offers shear rigidity and improves the flexural rigidity (Galletti *et al.* 2008). Fiber composites are generally used for the skins of the sandwich structure due to their low density and high mechanical performance (Shenhar *et al.* 1996). The laminates of fiber composite material, either of unidirectional or woven using glass or carbon, are widely used as face sheets materials for the sandwich structures

(Manalo *et al.* 2010, Tekalur *et al.* 2009). The demanded strength and stiffness features of the sandwich structures can be improved by altering the materials for the core and the skins (Daniel and Abot 2000). By means of analytical description, Finite Element Analysis (FEA) indicated that the stress was concentrated at the loading zone as well as supporting zone of the composite sandwich beams when it is subjected to bending loads (Lu *et al.* 2015). The failure modes of sandwich beams with aluminum honeycomb core and three different materials of woven fabric (glass – carbon – aramid) were investigated under static three-point bending by (Mines *et al.* 1994). The results displayed that the top skin compression failure of the sandwich beam was considered as the most common failure mode as compared to core shear or bottom tensile failure. Dai and Hahn (2003) investigated the effect of span length on the flexural behavior of sandwich beams with grain balsa wood core and E-glass composite skins with a stacking sequence of [0/45/90/-45/45/90/-45/0]. Higher shear strength was observed for the short span specimens, while the long span specimens were dominated by skin failure. Borsellino *et al.* (2004) performed compressive, shear, and flexural tests for the sandwich structure with different kinds of woven skin materials (Kevlar, glass and carbon fibers). The results showed that different skins extremely affect the fracture mechanism. Fan *et al.* (2007) investigated the mechanical behavior of the sandwich panels of Kagome lattice cores reinforced by T300 carbon fiber composite with stacking sequence of [0/±45/90]₂ under three-point bending, in-plane compression, and out-of-plane compression. The results revealed that the mechanical behavior of the sandwich

*Corresponding author, Ph.D.
E-mail: haziman@uthm.edu.my

structures is controlled by the debonding and buckling more than elastic deformation and core shear. Russo and Zuccarello (2007) studied the mechanical behavior of the sandwich structure of PVC foam core and fiber glass laminate skins (Randomly oriented) under three and four-point loading tests. The results summarized that the specimens with long span have failed as a result of the bottom skin tensile failure while the specimens with short span failed due to shear failure of the core. Gdoutos and Daniel (2008) investigated the flexural behavior of composite sandwich beams of a PVC closed-cell foam core and 8-ply unidirectional carbon/epoxy skins under three- and four-point bending. It was found that the failure modes of sandwich beams rely on the loading type, geometrical dimensions, and constituent materials. Manalo *et al.* (2010) investigated the flexural behavior of composite sandwich beams of glass fiber-reinforced polymer skins composites (2-ply of bi-axial) and modified phenolic core under four-point static bending test in edgewise and flatwise positions. The edgewise composite sandwich beams failed due to progressive failure of the skin while the flatwise composite sandwich beams failed due to skin compressive failure followed by skin-core debonding. On the other hand, Ferdous *et al.* (2017) proved that the vertical positions of phenolic core-glass fiber composite sandwich beams are suitable for shear dominated structures while the horizontal positions are desirable for flexural controlled structures. Fan *et al.* (2013) investigated the bending behavior of the sandwich panels of CFRP interlocked lattice core reinforced with two different thicknesses and sequences of T300 CFRP laminate, which are 0.5 mm of $[0/\pm 45/0]$ and 1.5 mm of $[\pm 45/0/90/0]_2$, respectively. The results revealed that the mechanical behavior of the sandwich structures was controlled by debonding failure. Fotsing *et al.* (2016) examined the effect of face sheet modification and core discontinuities of composite sandwich panels under three-point bending test. The results presented that the flexural properties of sandwich structures remain unchanged when discontinuities of 2 mm are introduced in the core, or small viscoelastic patches are inserted between face sheet plies. However, Selver and Kaya (2019) found that the flexural loads, strength and modulus of sandwich composites significantly increased after inserting of glass and carbon pins through extruded-polystyrene (XPS) foam core. Wang *et al.* (2018) studied the effects of the core thickness and density on the strength of composite sandwich panel made up aluminum honeycomb core and 4 layers of carbon fiber prepreg skins under three-point bending. The results revealed that the strength enhanced by increasing the thickness density of the core.

In general, many investigations have been performed and more are ongoing worldwide in the field of performance evaluation of fiber reinforced polymer (FRP) materials in their application as skin faces in a sandwich structure. The need for more optimized design methods cannot be overemphasized. In particular, the focus on "an ultralight low mass integrated with high performance face sheet material" has not been fully explored in the recent researches. The single ply of triaxial woven fabric (TWF) composite presented high performance and flexibility in the

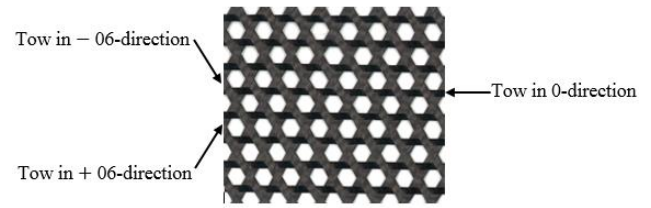


Fig. 1 TWF composite structure

company of hexagonal holes spread over the composite (see Fig. 1).

TWF uniformly carries the load in tension, bending, and shear (Kueh 2012, Kueh 2014), has good stiffness, strength and fracture properties (Xu *et al.* 2007, Al-Fasih *et al.* 2017, Al-Fasih *et al.* 2018), is highly flexible in the out-of-plane direction (Aoki *et al.* 2007), and has good impact behavior and low thermal sensitivity (Zhao and Hoa 2003, Xu *et al.* 2005). Therefore, the aforementioned good features of single ply TWF composite are worthwhile to be examined for application as high performing and low mass face skin material for composite sandwich structures.

The aim of this study is to investigate the flexural behavior of sandwich beams through the use of TWF composite as the novel proposed skin in comparison to that of conventional unidirectional type. The novel CFRP laminate skin of interest consists of TWF composite lamina and UD composite lamina. This study includes standard testing and numerical analysis of the sandwich beam under four-point flexural loads commonly experienced during normal loading of structures.

2. Experimental work

2.1 Description of material and specimens

Specimens for the experimental study were constructed in the form of SHC beam consisted of two CFRP face skins and aluminum honeycomb core with thickness, t_c , of 20 mm. Two material types of CFRP were considered for the skins: Stitched unidirectional (UD) carbon fiber composite T350 with a dry density of 300 g/m² and the triaxially woven (TW) fabric in 'basic weave' pattern consisting of 1000-filament in each T300 carbon fiber tow, which has a dry density of 100 g/m² (see Fig. 2).

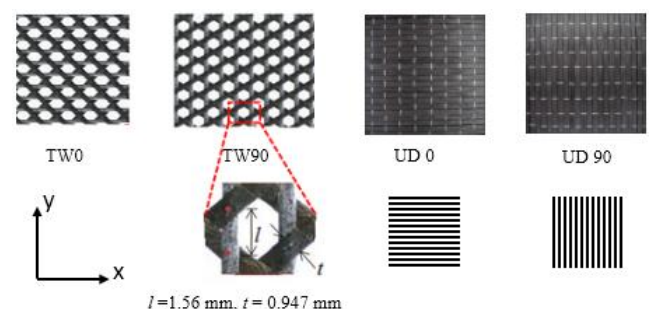


Fig. 2 Dry TWF with its highlighted unit cell and dry UD carbon fiber sheets

Table 1 Dimensions of the SHC beam and its aluminum honeycomb unit cell

Total length of beam, L_T (mm)	350
Width of beam, b (mm)	30
Length of inclined wall, h (mm)	3.536
cell size, l (mm)	3.0
Thickness of the inclined wall, t (mm)	0.064
Cell wall angle, θ	45°

Table 2 Details of SHC beam specimen for four-point loading flexural test

Specimen name	Materials stacking sequence	b (mm)	t_c (mm)	L (mm)	L_T (mm)	Density (kg/m ³)
UD0/90	[UD0/UD90/core/UD90/UD0]	30	20	300	350	225
TW0/UD0	[TW0/UD0/core/UD0/TW0]	30	20	300	350	184
TW0/UD90	[TW0/UD90/core/UD90/TW0]	30	20	300	350	184

The commercial epoxy resin, Epicoate 1006, and hardener with the 5:3 proportions, were employed as the epoxy matrix. The geometrical descriptions of the beam and the hexagonal unit cell of the aluminum honeycomb core are shown in Fig. 3 and numerically summarized in Table 1.

Three samples for each UD0/90, TW0/UD0, and TW0/UD90 SHC beam were assembled according to the dimensions and the layers staking sequences as presented in Table 2, in which the UD0/90 carbon fiber composite (conventional skin) were compared with two arrangements of the novel skins, which were TW0/UD0 and TW0/UD90. UD0/90 carbon fiber composite was made of plies of stitched UD with the stacking sequence of [0/90] with the nominal thickness of 0.8 mm and a density of 1000 g/m², while TW0/UD0 carbon fiber composite was made up of 0°-direction single ply TW and 0°-direction single ply UD with a nominal thickness of 0.6 mm and a density of 611 g/m²; and TW0/UD90 carbon fiber composite was made of 0°-direction single ply TW and 90°-direction single ply UD with a nominal thickness of 0.6 mm and a density of 611 g/m². Based on the laminate densities, it is noted that both laminates of TW0/UD0 and laminates of TW0/UD90 are 39 % lighter than the laminates of UD0/90. On the other hand, the overall densities of SHC beams are listed in Table 2.

2.2 Manufacturing process of specimens

In the assembling process of the SHC beam, an equal distribution of the bonding resin (5:3 Epicoate1006 to hardener) was applied on the skin-to-core interfaces by hand lay-up, and then the aluminum honeycomb core was sandwiched immediately between the two skins. The vacuum bagging method was employed at a pressure of 0.0827 MPa for the complete sandwich structure lay-up for a period of 4 h to eliminate air. The composite was then cured at the room temperature of 25°C for 24 h. Then, for the strain measurement of the laminate skins during the flexural test, two strain gages were attached longitudinally

to the mid-span of the top most and bottom most laminate skin surfaces.

2.3 Test set-up and procedure

Tensile, compression, shear coupon tests were experimentally conducted to determine the mechanical characteristics of the CFRP materials in accordance with ASTM D3039/D3039M (ASTM 2008), ASTM D3410/D3410M (ASTM 2008) and ASTM D3518/D3518M (ASTM 2001), respectively. Table 3 shows the mechanical properties of the single ply UD T350/EP-6001 and single ply TW T300/EP-6001, and Table 4 shows the average values with considering the linear approximation of the elastic modulus, peak stress and strain of the UD0/90, TW0/UD0, and TW0/UD90 composite laminate skins.

The static flexural test of SHC beam was performed in accordance with the ASTM C393 (ASTM 2002). Fig. 4 shows the schematic illustration and actual flexural test set-up of the SHC beam. The flexural tests were carried out using the Universal Instron machine 5567 with 30 kN load cell with a loading rate of 3 mm/min. The load was applied at $L/4$ and at the $3L/4$ points of the span.

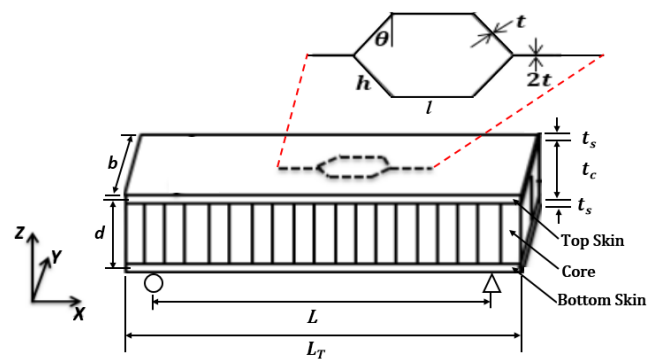


Fig. 3 Schematic of the SHC beam and the honeycomb unit cell geometry

Table 3 Mechanical Properties of UD T350/EP-6001 and TW T300/EP-6001

Property	UD	TWF
Density, ρ (kg/m ³)	998	221.5
Longitudinal stiffness, E_1 (MPa)	123387	13126
Transverse stiffness, E_2 (MPa)	8372	7608
Poisson's ratio, ν_{12}	0.319	0.32
In-plane shear modulus, G_{12} (MPa)	4278	2798
Out-of-plane shear modulus, G_{13} (MPa)	4278	2798
Out-of-plane shear modulus, G_{23} (MPa)	2968	2,859
Longitudinal tensile strength, X_t (MPa)	926	143
Longitudinal compressive strength, X_c (MPa)	345	41.5
Transverse tensile strength, Y_t (MPa)	8	65
Transverse compressive strength, Y_c (MPa)	57	5.2
Longitudinal shear strength, S_t (MPa)	19.45	11.5
Transverse shear strength, S_c (MPa)	19.45	11.5

Table 4 Characteristics of the CFRP laminate skins

Test/standard	Property	UD0/90	TW0/UD0	TW0/UD90
Tensile/ ASTM standard D3039/D3039M-08	Elastic modulus (MPa)	113,550	118,440	17920
	Peak stress (MPa)	993	1,057	159
	Strain at peak (microstrains)	9,743	8,659	10,148
Compression/ ASTM standard D3410/D3410M-08	Elastic modulus (MPa)	89,980	59,014	13,414
	Peak stress (MPa)	416	373	105
	Strain at peak (microstrains)	10842	10740	10930
Shear/ ASTM standard D3518/D3518M-01	Elastic modulus (MPa)	4277	4220	4175
	Peak stress (MPa)	19.45	24.6	23.15
	Strain at peak (microstrains)	6981	5662	5760

Linear variable displacement transducer (LVDT) was placed in the middle part of the fixture to evaluate the mid-span displacement. The LVDT and uni-axial strain gages were connected to the data logger to evaluate the mid-span displacement and the longitudinal strain, respectively, during loading until final failure. Before each test, the loading pins were set to almost touching the top surface of the SHC beam specimen and the LVDT was set to touch the bottom surface of the SHC beam at the mid-span. The applied load, displacement, and strains were recorded. The test was stopped after the failure of the SHC beams was observed. The flexural stress, σ , under four-point bending for each applied load, which carried by the surface fibers of the top and bottom skins of the SHC beam, was calculated according to the expression of Caprino and Teti (1989)

$$\sigma = \frac{PL(t_s + 0.5t_c)}{4bt_s t_c^2} \quad (1)$$

where P is the applied load, L is the supporting span, t_s is the skin thickness, t_c is core thickness and b is the width of the beam.

3. Finite element modeling of composite sandwich structural behavior

The finite element modeling (FE) using the commercial software ABAQUS 6.13/standard (ABAQUS 2013) was developed to predict the behavior, failure modes and the ultimate capacity of the SHC beams. The specimen and the loading set-up was simulated as identically as possible with the actual experimental conditions to have a reliable result. Four-point static bending behavior of the SHC beam was performed by developing a 3D finite-element model in the ABAQUS/standard domain. The model included: load parts, support parts, and all composite of SHC beam. The boundary conditions of the model were applied as a constraint at the midspan of the top and bottom skins and at

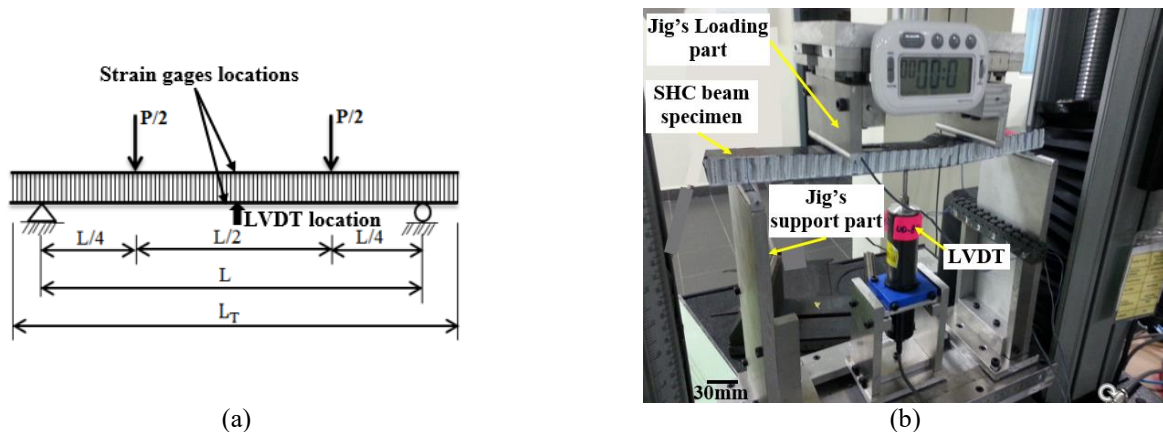


Fig. 4 (a) Schematic illustration of the flexural test of composite sandwich structures and (b) Actual test set-up for SHC beam specimen

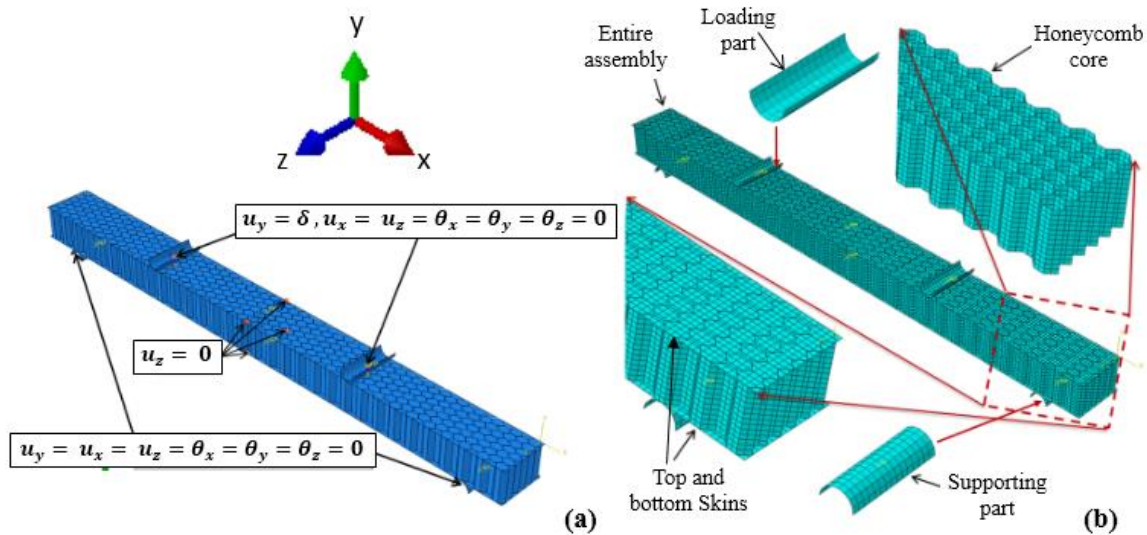


Fig. 5 (a) A numerical model of the SHC beam with boundary conditions and (b) Numerical meshes for all parts of the SHC beam specimen

the reference points of the supporting and loading parts as shown in Fig. 5(a).

The support and load spans were 300 mm and 150 mm, respectively. The skins were modeled as elastic materials, defined with properties established from the coupon tests as listed in Table 3. The aluminum honeycomb core was modeled as an elastic-plastic material following the work of Ivañez and Sanchez-Saez (2013). The Young's modulus and Poisson's ratio of the aluminum foil were 69000 MPa and 0.33, respectively. The surface-based tie constraint was adopted to define the adhesive bonding between both skins and core to simulate a perfect bonding between them. Surface-to-surface contact was defined with the friction coefficient of 0.1 between the outer surface of both supporting and loading parts with the surface of skins at the region beneath the supporting and loading parts only.

Three types of model were developed to represent UD0/90, TW0/UD0, and TW0/UD90 SHC beams, respectively. The top and bottom skins, as well as the core, were meshed using 4-node shell element (S4) without the reduction integration. The UD0/90 CFRP skins were modeled to have a shell-composite section with a stacking sequence of [0/90] with 0.4 mm thickness for each layer. The TW0/UD0 CFRP skins were modeled to have a shell-composite section with 0°-direction for both TW and UD materials with thicknesses of 0.167 mm and 0.4 mm, respectively, while shell-composite section with 0°-direction and 90°-direction material orientation were considered for TW and UD material, respectively, to represent the modeling of the TW0/UD90 CFRP skins. The honeycomb core foils were modeled to have a shell-homogenous section with a shell thickness of 0.1 mm. The supporting and loading parts (10 mm diameter) were then discretized with the discrete rigid element (R3D4) (see Fig. 5(b)). The refinements of the mesh were carried out until the

Table 5 Summary of test results of SHC beams under four-point loading

Beam skin type	Result	P_u (N)	P_u /wt ratio	δ_u (mm)	δ_{bu} (MPa)	Bottom-face ϵ_u (microstrains)	Top-face ϵ_u (microstrains)
UD0/90	Average	4,375	85	6.44	369	5,263	4,880
	S.D	64	3.2	0.25	5.4	491	386
	C.V (%)	1.4	1.1	3.9	1.4	9.3	7.9
TW0/UD0	Average	3,803	89	5.45	385	4,957	4,992
	S.D	65	4.3	0.24	6.7	250	456
	C.V (%)	17	1.3	4.4	18	12.6	9.1
TW0/UD90	Average	1,433	33	14.14	158	12,798	13,060
	S.D	85	3.8	0.263	9.44	707	526
	C.V (%)	6	1.5	1.8	6	5.5	4

optimal convergence plot was achieved. An average of 1.7 mm element size for the skins, 2.0 mm for supporting and loading parts, and 1.5 mm for the shell elements of aluminum honeycomb were considered with the total number of 38,416 elements for the finalized models.

Analysis of the models was conducted using the nonlinear geometry static step. The failure of the SHC beam models was defined as when the maximum strength in the elements, either in terms of the maximum tensile, or compressive, shear strength of the material, were exceeded. The deflection and bending stress-strain relationships at the top-most and bottom-most shell elements at the mid-span results were plotted and then compared with those of the experimental for the SHC beams for verification purposes.

4. Results and discussion

4.1 Load-deflection behavior

The load-displacement curves of the SHC beam specimens are shown in Fig. 6. In the plot, FE added to the specimen codes at the end to represent the finite element specimens. It is noticed that the UD0/90 SHC beam specimens failed at the average maximum load of 4375 N with the average mid-span deflection of 6.44 mm. The load increased linearly with deflection, then sudden failure was observed after the maximum failure load point. After the peak, the load dropped to almost 83% of the average maximum applied load. The dropping of the load due to the total failure of the skin material resulted in total stiffness reduction of the SHC beams. The load-deflection behavior of TW0/UD0 SHC beam specimens showed a linear behavior in stiffness until the maximum average load of around 3803 N with average mid-span displacement of 5.4 mm. When the specimens failed, a gradual drop in the loads was observed due to core shear followed by the compressive skin failure. The load reduced to 80% of the maximum applied load. This reduction of the load was due to a total failure of the skin resulting in the stiffness reduction. This suggests that the skin contributed to the total stiffness of the SHC beam. After the dropping of the load,

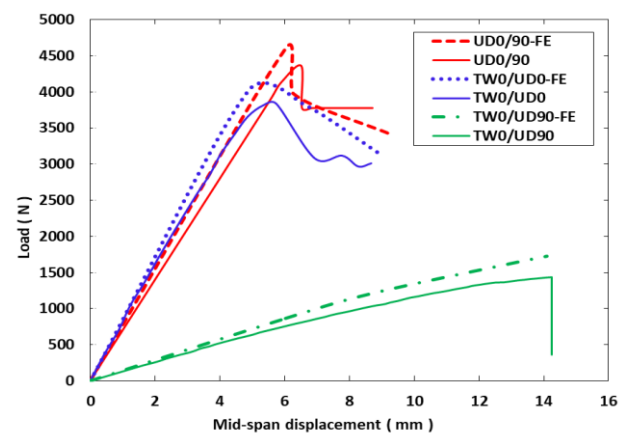


Fig. 6 Load and mid-span displacement relationship of UD0/90, TW0/UD0, and TW0/UD90 SHC beam specimens

the specimen continued to bear the load without surpassing the prior peak load as the core and bottom skin were the remaining components carrying the load. The specimens of TW0/UD90 SHC beam exhibited a linear behavior up to a deflection of approximately 6.6 mm. At larger deflections, a small extent of nonlinearity occurred with stiffness softening up to failure. This behavior can be attributed to the flexible nature of the aluminum honeycomb core before the initiation of compressive failure of the top skin. When the skin failed, a sudden drop in the load was witnessed and the specimen failed consequently.

The average of the maximum vertical mid-span deflection was 14.14 mm at a maximum average failure load of 1433 N.

In general, UD0/90 and TW0/UD0 SHC beam specimens have almost the same load-deflection behavior, resulting in fairly the same stiffnesses of 679 N/mm and 697 N/mm, respectively. This is due to small differences in tensile and compressive stiffnesses of the UD0/90 and TW0/UD0 laminate skins as found from the coupon tests as shown in Table 4. On the other hand, TW0/UD90 SHC beam specimens deflected more than twice that of TW0/UD0 SHC beam specimens under the same level of

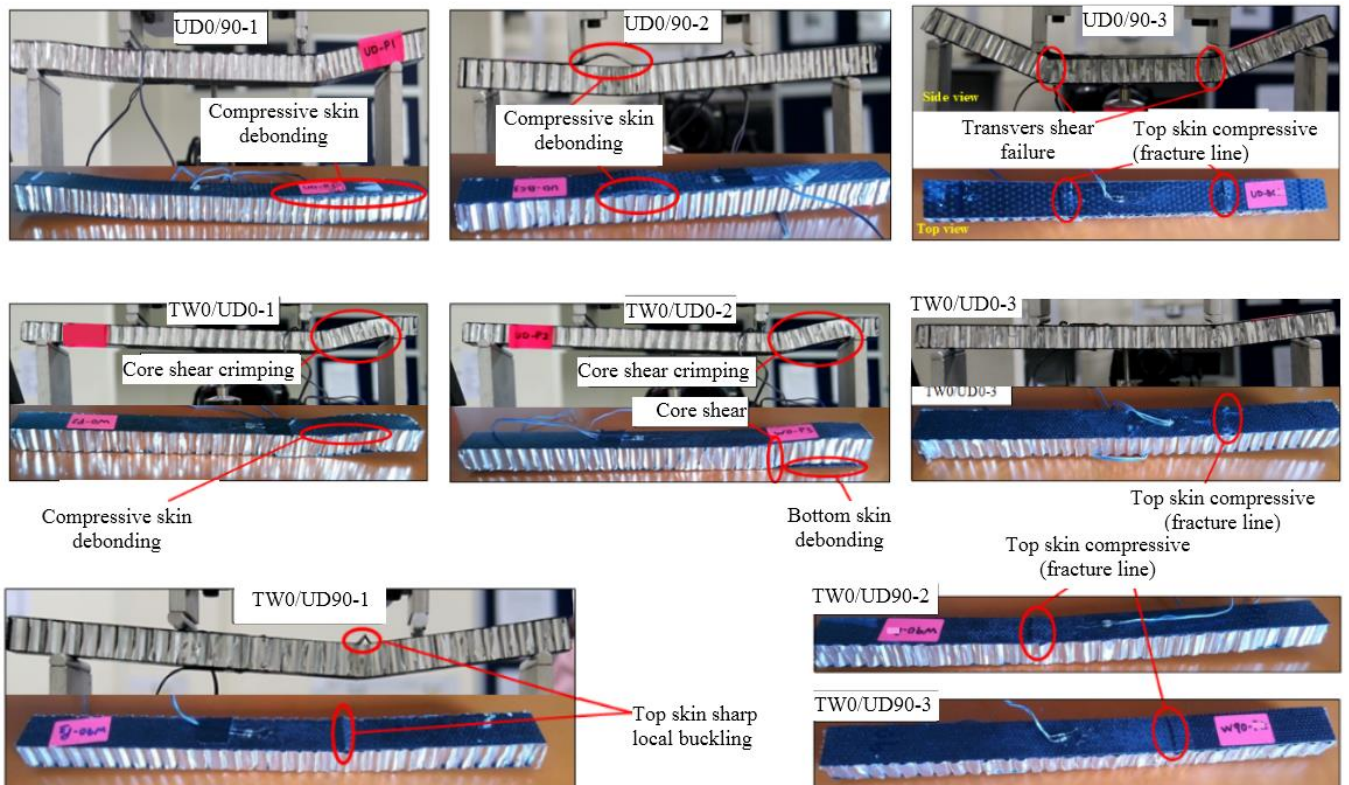


Fig. 7 Failure modes of SHC beam specimens

the applied load. This is due to the significant contribution of the orientation of the fibers of UD lamina along the axis of the beam on the flexural stiffness of the TW0/UD0 laminate skin compared to its low contribution in the transverse direction of TW0/UD90 laminate, and resulting in significant increases the flexural stiffness of the overall TW0/UD0 SHC beam.

4.2 Stress-strain behavior of SHC beams

The flexural stresses were determined for each applied load according to Eq. (1) in Section 2.3, while the tensile and compressive strains were evaluated from the attached strain gages at the mid-span of bottom and top of the SHC beams specimens. Table 5 summarizes the average values and its standard deviation, S.D, and coefficient of variation, C.V, for the maximum failure load (P_u), maximum failure load /weight ratio, P_u/wt , deflection, (δ_u), at the point of maximum failure load, maximum flexural stress (σ_{bu}) and the mid-span strain (ϵ_u) at the point of the maximum failure load of the bottom and top skins. For all specimen types, according to the strain of the top and bottom skins, the skins in compression behaved slightly stiffer than in tension. This implies that the assumption of the strains' compatibility throughout the depth of the SHC beam section is valid, that is, deformations at the top and bottom are mutually symmetrical. This is attributed to the symmetrical stacking sequence of materials from top to bottom (see Table 2 in Section 2.1). These stress and strain levels were significantly lower than those of the carbon fiber composite

skins established from the test of the laminate coupons (listed in Table 4, Section 2.3), which is attributed to observed failure mode due to the different loading.

According to the results, the TW0/UD0 SHC beam is better than the UD0/90 SHC beam due to its 5% higher P_u/wt ratio, making it the best arrangement as the skins for the sandwich structure, although P_u of the TW0/UD0 SHC beam is a 13% lower than that of UD0/90 SHC beam due to less fiber carrying the applied load at the loading edges.

The maximum variation in P_u , δ_u , σ_{bu} and ϵ_u values for all specimens is less than 20%. This outcome demonstrates the coherent manufacturing of the SHC beams, where the experimental techniques were performed within an acceptable margin of error.

4.3 Failure behavior

The SHC beam specimens generally failed under four-point bending in a brittle manner due to three types of failure modes, which are premature debonding failure between the skin and core, core shear or core crimping, and top compressive skin. Fig. 7 displayed that UD0/90-1 and UD0/90-2 SHC beam specimens failed due premature compressive skin debonding failure observed close to one loading point due to the nature of very small bonded area of the honeycomb cross section to compressive skin debonding failure mode. However, UD0/90-3 specimen failed due to symmetric transverse core shear failure followed by a compressive failure of the top compressed skin face underneath the loading points. On the other hand,

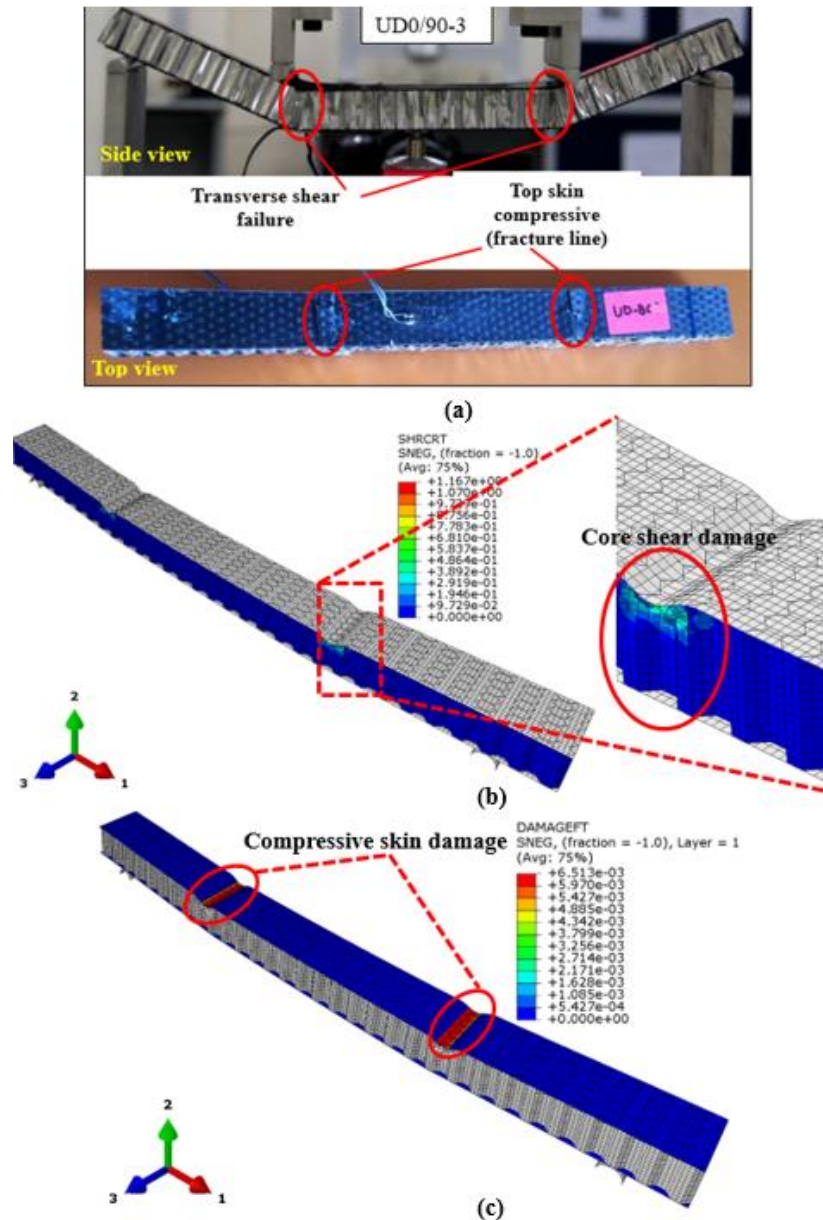


Fig. 8 Comparison of failure mechanisms between the experimental and numerical model of UD0/90 SHC beam specimen: (a) experimental specimen (b) shear damage from the FE model (c) compressive skin damage from FE model

TW0/UD0-1 SHC beam specimen failed due to core shear crimping followed by debonding of top skin at the right support point. Similarly, TW0/UD0-2 SHC beam specimen failed due to core shear crimping followed by successive debonding of the bottom skin at the right support point.

However, the specimen TW0/UD0-3 failed due to compressive failure of the top face, but only underneath one point-load location. Furthermore, the TW0/UD90 SHC beam specimens were controlled by top compressive skin failure due to local buckling of skin which resulted in a fracture line close to the loading points, in which TW0/UD90-1 and TW0/UD90-2 specimens failed due to compressive skin failure of sharp local buckling between the loading points region. These failure modes were observed by (Daniel *et al.* 2002, Lingaiah and Suryanarayana 1991) for the specimens of the composite

sandwiches of fiberglass reinforced plastic laminates with an aluminum honeycomb core, which were tested under four-point loading, and it is similar to the observation of Belingardi *et al.* (2007) for the static loading of the undamaged specimen of honeycomb composite sandwich beams. Likewise, the specimen TW0/UD90-3 failed due to compressive failure of the top face, but only underneath one point-load location.

To sum up, the UD0/90 and TW0/UD0 SHC beam specimens were dominated by the core shear or core crimping failure mode, while the TW0/UD90 SHC beam specimens were controlled by the compressive failures of the top skin, which resulted in fracture line (parallel to the width direction of the specimen) with no visible failure of the bottom skin under tension. Thus, in the case of exception of the premature debonding failure mode, it is

proved that the UD0/90 and TW0/UD0 laminates types have better compressive failure resistance prior the core shear failure occurring due to their high stiffness compared to TW0/UD90 laminate skin.

4.4 Numerical FE and experimental comparison

The overall comparison between FE numerical method and experimental tests of the SHC beams under four-point static bending in terms of the load-midspan deflection curves (see Fig. 6) indicated that the FE numerical approach can predict the load-deflection behavior of the SHC beams satisfactorily. A good agreement between the FE numerical and the experimental up to the final failure state was observed. The difference between the FE and the experimental results in terms of maximum failure load is only 12% for the UD0/90 SHC beam specimens and 15% for the TW0/UD0 beam specimens. However, the difference is as high as 27% for the TW0/UD90 specimens. The reason for this could be due to the weak tensile and compression stiffnesses of TW0/UD90 laminate skins compared to that of UD0/90 and TW0/UD0 laminate skins as shown in Section 2.3, Table 4. This small disagreement between FE numerical method and experimental tests could be due to the dimensions' variants of the experimental SHC beam specimens. According to the observation at the maximum stresses where the core and the skin of the SHC beam would potentially fail, the FE numerical model successfully predicted the behavior and failure mechanisms of the experimental test for SHC beams as shown in Fig 8, albeit with lesser cost and time compared to those of experiments.

5. Conclusions

The flexural behavior and failure mechanisms of the SHC beam reinforced by the novel skins of TW0/UD0 or TW0/UD90 were compared experimentally and numerically with those reinforced with UD0/90 conventional skins under four-point loading. The load-deflection and stress-strain relationships showed a significant similarity between the TW0/UD0 and UD0/90 SHC beams in terms of strength and stiffness, although the former was 39% lighter. This is due to the equality of TW0/UD0 and UD0/90 laminate skins in the tensile, compression, shear, and flexural stiffnesses and strength (in coupon test results), which contributed to the overall behavior of the SHC beam. On the other hand, the TW0/UD90 SHC beam specimens showed 70% lower efficiency than those of UD0/90 SHC beams. Thus, the flexural stiffness increased due to the stacking sequence effect, suggesting that the application of the TW/UD composite laminate in the TW0/UD0 design is better than TW0/UD90 to carry high tensile and compressive stresses.

According to the experimental observation, the SHC beam specimens generally failed in a brittle manner. Note that the UD0/90 and TW0/UD0 SHC beam specimens were dominated by the core shear or core crimping failure mode, while the TW0/UD90 SHC beam specimens were controlled by the compressive failures of the top skin,

resulting in fracture line (parallel to the width direction of the specimen) with no visible failure of the bottom skin under tension. Thus, in the case of exception of the premature debonding failure mode, it is indicated that the UD0/90 and TW0/UD0 laminates types have better compressive failure resistance prior the core shear failure occurring due to their high stiffness compared to TW0/UD90 laminate skin. On the other hand, the FE modeling agreed very well with the experimental outcomes, giving confidence in the validity of the modeling assumption.

In general, the results consistently showed the high potential of the TW0/UD0 composite laminate as the skin material for the sandwich honeycomb composite beam. Accordingly, the expected research impact of TWF composite application as the skin for the sandwich structure is a successful development of a structural system of sandwich beams that can effectively withstand flexural loads with greater strength and stiffness, useful for any industrial and scientific community in need of lightweight and tough structures with wavy members.

References

- ABAQUS Version 6.13 (2013), Analysis User's Guide, Dassault Systems.
- Al-Fasih, M.Y., Kueh A.B.H., Abo Sabah, S.H. and Yahya, M.Y. (2018), "Tow waviness and anisotropy effects on mode II fracture of triaxially woven composite", *Steel Compos. Struct.*, **26**(2), 241-253. <https://doi.org/10.12989/scs.2018.26.2.241>.
- Al-Fasih, M.Y., Kueh A.B.H., Abo Sabah, S.H. and Yahya, M.Y. (2017), "Influence of tows waviness and anisotropy on effective mode I fracture toughness of triaxially woven fabric composites", *Eng. Fract. Mech.*, **182**, 521-536. <https://doi.org/10.1016/j.engfracmech.2017.03.051>.
- Aoki, T., Yoshida, K. and Watanabe, A. (2007), "Feasibility study of triaxially-woven fabric composite for deployable structures", *Proceedings of the 48th AIAA/ASME/ASCE/AHS/ASC Structures, Structural Dynamics and Materials Conference*, Honolulu, HI, USA, April. <https://doi.org/10.2514/6.2007-1811>.
- ASTM C393 (2002), Standard Test Method for Flexural Properties of Sandwich Constructions; The American Society for Testing and Materials, USA.
- ASTM D3039/D3039M (2008), Standard Test Method for Tensile Properties of Polymer Matrix Composite Materials; ASTM International, West Conshohocken, PA, USA.
- ASTM D3410/D3410M (2003), Standard Test Method for Compressive Properties of Polymer Matrix Composite Materials with Unsupported Gage Section by Shear Loading; ASTM West Conshohocken, PA USA.
- ASTM D3518/D3518M (2001), Standard Test Method for in-Plane Shear Response of Polymer Matrix Composite Materials by Tensile Test of a 45 Laminate; American Society of Testing Materials, USA.
- Belingardi, G., Martella, P. and Peroni, L. (2007), "Fatigue analysis of honeycomb-composite sandwich beams", *Compos. Part A Appl. Sci. Manuf.*, **38**(4), 1183-1191. <https://doi.org/10.1016/j.compositesa.2006.06.007>.
- Belouettar, S., Abbadi, A., Azari, Z., Belouettar, R. and Freres, P. (2009), "Experimental investigation of static and fatigue behaviour of composites honeycomb materials using four point bending tests", *Compos. Struct.*, **87**(3), 265-273. <https://doi.org/10.1016/j.compstruct.2008.01.015>.

- Borsellino, C., Calabrese, L. and Valenza, A. (2004), "Experimental and numerical evaluation of sandwich composite structures", *Compos. Sci. and Technol.*, **64**(10-11), 1709-1715. <https://doi.org/10.1016/j.compscitech.2004.01.003>.
- Caprino, G. and Teti, R. (1989), *Sandwich Structures: Handbook*, II Prato, Padua, Italy.
- Dai, J. and Hahn, H.T. (2003), "Flexural behavior of sandwich beams fabricated by vacuum-assisted resin transfer molding", *Compos. Struct.*, **61**(3), 247-253. [https://doi.org/10.1016/S0263-8223\(03\)00040-0](https://doi.org/10.1016/S0263-8223(03)00040-0).
- Daniel, I.M. and Abot, J.L. (2000), "Fabrication, testing and analysis of composite sandwich beams", *Compos. Sci. Technol.*, **60**(12-13), 2455-2463. [https://doi.org/10.1016/S0266-3538\(00\)00039-7](https://doi.org/10.1016/S0266-3538(00)00039-7).
- Daniel, I.M., Gdoutos, E.E., Wang, K.A. and Abot, J.L. (2002), "Failure modes of composite sandwich beams", *Int. J. Damage Mech.*, **11**(4), 309-334. <https://doi.org/10.1106/105678902027247>.
- Fan, H.L., Meng, F.H. and Yang, W., (2007), "Sandwich panels with Kagome lattice cores reinforced by carbon fibers", *Compos. Struct.*, **81**(4), 533-539. <https://doi.org/10.1016/j.compstruct.2006.09.011>.
- Fan, H., Yang, L., Sun, F. and Fang, D., (2013). "Compression and Bending Performances of Carbon Fiber Reinforced Lattice-Core Sandwich Composites." *Compos. Part A Appl. Sci. Manuf.*, **52**, 118-25. <https://doi.org/10.1016/j.compositesa.2013.04.013>.
- Ferdous, W., Manalo, A. and Aravinthan, T. (2017), "Effect of beam orientation on the static behaviour of phenolic core sandwich composites with different shear span-to-depth ratios", *Compos. Struct.*, **168**, 292-304. <https://doi.org/10.1016/j.compstruct.2017.02.061>.
- Fotsing, E.A., Leclerc, C., Sola, M., Ross, A. and Ruiz, E. (2016), "Mechanical properties of composite sandwich structures with core or face sheet discontinuities", *Compos. Part B Eng.*, **88**, 229-239. <https://doi.org/10.1016/j.compositesb.2015.10.037>.
- Fotsing, E.A., Leclerc, C., Sola, M., Ross, A. and Ruiz, E. (2008), "Theoretical design and analysis of a honeycomb panel sandwich structure loaded in pure bending", *Eng. Fail. Anal.*, **15**(5), 555-562. <https://doi.org/10.1016/j.engfailanal.2007.04.004>.
- Gdoutos, E.E. and Daniel, I.M. (2008), "Failure Modes of Composite Sandwich Beams." *Theor. Appl. Mech.*, **35**(1-3), 105-18. <https://doi.org/10.2298/TAM0803105G>.
- He, M. and Hu, W., (2008). "A study on composite honeycomb sandwich panel structure", *Mater. Des.*, **29**(3), 709-713. <https://doi.org/10.1016/j.matdes.2007.03.003>.
- Ivañez, I. and Sanchez-Saez, S. (2013), "Numerical modelling of the low-velocity impact response of composite sandwich Beams with honeycomb core", *Compos. Struct.*, **106**, 716-723. <https://doi.org/10.1016/j.compstruct.2013.07.025>.
- Kueh, A.B.H. (2012), "Fitting-free hyperelastic strain energy formulation for triaxial weave fabric composites", *Mech. Mater.*, **47**, 11-23. <https://doi.org/10.1016/j.mechmat.2012.01.001>.
- Kueh, A.B.H. (2014), "Size-influenced mechanical isotropy of singly-ply triaxially woven fabric composites", *Compos. Part A Appl. Sci. Manuf.*, **57**, 76-87. <https://doi.org/10.1016/j.compositesa.2013.11.005>.
- Lingaiah, K. and Suryanarayana, B.G. (1991), "Strength and stiffness of sandwich beams in bending", *Exp. Mech.*, **31**(1), 1-7. <https://doi.org/10.1007/BF02325715>.
- Lu, C., Zhao, M., Jie, L., Wang, J., Gao, Y., Cui, X. and Chen, P. (2015), "Stress distribution on composite honeycomb sandwich structure suffered from bending load", *Procedia Eng.*, **99**, 405-12. <https://doi.org/10.1016/j.proeng.2014.12.554>.
- Manalo, A.C., Aravinthan, T., Karunasena, W. and Islam, M.M. (2010), "Flexural behaviour of structural fibre composite sandwich beams in flatwise and edgewise positions", *Compos. Struct.*, **92**(4), 984-995. <https://doi.org/10.1016/j.compstruct.2009.09.046>.
- Mines, R.A.W., Worrall, C.M. and Gibson, A.G. (1994), "The static and impact behaviour of polymer composite sandwich beams", *Composites.*, **25**(2), 95-110. [https://doi.org/10.1016/0010-4361\(94\)90003-5](https://doi.org/10.1016/0010-4361(94)90003-5).
- Russo, A. and Zuccarello, B. (2007), "Experimental and numerical evaluation of the mechanical behaviour of GFRP sandwich panels", *Compos. Struct.*, **81**(4), 575-586. <https://doi.org/10.1016/j.compstruct.2006.10.007>.
- Selver, E. and Kaya, G. (2019), "Flexural properties of sandwich composite laminates reinforced with glass and carbon Z-pins", *J. Compos. Mater.*, **53**(10), 1347-1359. <https://doi.org/10.1177/0021998318800146>.
- Shenhar, Y., Frostig, Y. and Altus, E. (1996), "Stresses and failure patterns in the bending of sandwich beams with transversely flexible cores and laminated composite skins", *Compos. Struct.*, **35**(2), 143-152. [https://doi.org/10.1016/0263-8223\(96\)00016-5](https://doi.org/10.1016/0263-8223(96)00016-5).
- Tekalur, S.A., Bogdanovich, A.E. and Shukla, A. (2009), "Shock loading response of sandwich panels with 3-D woven E-glass composite skins and stitched foam core", *Compos. Sci. Technol.*, **69**(6), 736-753. <https://doi.org/10.1016/j.compscitech.2008.03.017>.
- Wang, J., Shi, C., Yang, N., Sun, H., Liu, Y. and Song, B., (2018), "Strength, stiffness, and panel peeling strength of carbon fiber-reinforced composite sandwich structures with aluminum honeycomb cores for vehicle body", *Compos. Struct.*, **184**, 1189-1196. <https://doi.org/10.1016/j.compstruct.2017.10.038>.
- Xu, D., Ganesan, R. and Hoa, S.V. (2007), "Buckling analysis of tri-axial woven fabric composite structures subjected to bi-axial loading", *Compos. Struct.*, **78**(1), 140-152. <https://doi.org/10.1016/j.compstruct.2005.08.021>.
- Xu, D., Ganesan, R. and Hoa, S.V. (2005), "Buckling analysis of tri-axial woven fabric composite structures. Part I: non-linear finite element formulation", *Compos. Struct.*, **67**(1), 37-55. <https://doi.org/10.1016/j.compstruct.2004.01.004>.
- Zhao, Q.I. and Hoa, S.V. (2003), "Thermal deformation behavior of triaxial woven fabric (TWF) composites with open holes", *J. Compos. Mater.*, **37**(18), 1629-1649. <https://doi.org/10.1177/0021998303035192>.

CC